



Pseudo-ductile behaviour of fibrous composite Z-pins

E. Santana de Vega^{*}, G. Allegri, B. Zhang, I. Hamerton, S.R. Hallett

Bristol Composites Institute, Queen's Building, University of Bristol, University Walk, Bristol BS8 1TR, UK

ARTICLE INFO

Keywords:

A. Polymer-matrix composites (PMCs)
B. Delamination
E. Pultrusion
Z-pins

ABSTRACT

This paper describes the development and characterisation of a novel type of composite Z-pin able to accommodate large deformation without exhibiting fibre failure. Three types of pseudo-ductile Z-pins are fabricated by means of micro-pultrusion of polybenzoxazole (PBO) fibres. Namely, unidirectional PBO fibre (uPBO) Z-pins in combination with a ductile (uPBO/DCT) and a brittle (uPBO/BT) matrix system are developed, together with a twisted PBO fibre Z-pin in combination with a ductile matrix (tPBO/DCT). Single pin bridging tests are carried out across the full mode mixity range from mode I ($\Phi = 0$) to mode II ($\Phi = 1$). The tests reveal that uPBO-based pins are able to pull out throughout the full mode mixity range, regardless of the ductility of the pin matrix. uPBO/DCT pins exhibit a 20-fold increase in energy dissipation per pin than traditional carbon fibre/bismaleimide (CF/BMI) pins at load mode mixities higher than $\Phi = 0.9$. The mode I behaviour of all pins considered is comparable. All PBO pins exhibit an apparent delamination toughness enhancement superior to CF/BMI at mode mixities above $\Phi = 0.2$, with a ductile matrix increasing the average energy dissipated per pin by a further 2–8 %.

1. Introduction

Z-pinning is a widely used method of composites through-thickness reinforcement, specifically designed to be introduced into uncured prepreg-based composite laminates. Although there are other methods of orthogonally reinforcing a composite such as stitching [1], tufting [2] or the use of more complex 3D preforms [3], these typically rely on dry fibre reinforcement and are not as suited for structures which require the use of prepreg. The earliest use of Z-pinning technology dates back to the 1970s [4] and was further developed during the 1980s [5,6]. Since then, numerous research groups have studied the effectiveness of different Z-pin types in suppressing interlaminar crack formation and propagation, as captured by some key review papers [7–9].

Z-pins are typically either metallic or composite rods of small diameter (under 0.6 mm), although their structure and composition may vary. The most widely accepted and studied pin types are those made from a high strength metal such as steel or titanium or a composite of carbon fibre and a bismaleimide (BMI) resin. The use of high strength and ductile metals as Z-pins has numerous advantages as they can excel at mode II delamination suppression. The ductility of steel ensures the pin is able to bridge the interlaminar crack and oppose the shear displacement up to full pin pull-out [10,11]. Their effectiveness in suppressing mode I delamination is less pronounced, as they tend to exhibit low pull-out traction forces when the primary displacement is

crack opening. Surface modifications and treatments [12,13] can be used to promote the laminate-pin bond, albeit other issues remain such as galvanic corrosion and environmental susceptibility. In comparison, carbon fibre (CF) based composite Z-pins offer a superior delamination bridging performance during mode I dominated crack propagation, but they offer modest mode II improvement [14,15]. Carbon fibre/bismaleimide (CF/BMI) pins, the most common composition, are unable to pull out at mode mixities above 30 % mode II [16,17]. They instead fail through transverse rupture.

In recent years, there has been a focus in understanding how the structure of composite Z-pins affects their performance. The effect of pin diameter [14], length [18,19] and even cross-sectional geometry [20–22] on in-plane and interlaminar behaviour has been well documented. Similarly, surface modifications to CF pins such as notches [23], coatings [24], and chemical treatments [25] have all been reported methods of improving the existing pull-out behaviour of composite Z-pins. However, all these methods have failed to increase the mode mixity band at which the pin failure mode transitions from pull-out to rupture. Previous work by the authors of this paper [26] identified how the use of a ductile matrix can increase the position of this pull-out to rupture transition, up to 55 % mode II, but rupture still occurs above this mode mixity.

This study presents the use of an alternative high strength and high elongation fibrous reinforcement to produce pseudo-ductile composite

^{*} Corresponding author.

E-mail address: eduardo.santanadevega@bristol.ac.uk (E. Santana de Vega).

Z-pins which can pull out from the laminate regardless of loading mode mixity. The term of pseudo-ductile refers to their ability to bend and permanently deform over small radii without fibre failure, resembling the behaviour of ductile metallic pins. This contrasts with the typical brittle failure of composite CF/BMI pins when subjected to a shear load or a small a bending radius. The manufacturing and testing considerations are first identified, followed by evaluation of the characteristics of these novel pseudo-ductile Z-pins. Three types of Z-pins are discussed, *i. e.* two-unidirectional PBO fibre (uPBO) Z-pins with matrices of different ductility and a twisted PBO fibre (tPBO) pin.

2. Materials and methods

2.1. Materials

Cyanate ester and BMI monomers were supplied by Lonza AG (Visp, Switzerland) and Evonik Industries (Hannau-Wolfgang, Germany) respectively. E-glass/913 epoxy prepreg was supplied by Hexcel UK. Poly(*p*-phenylene-2,6-benzobisoxazole) (PBO) fibre was supplied by Toyobo (Japan). Epoxy resin and hardener (Araldite©LY3508 + Aradur©22962 [27]) were supplied by Huntsman Corporation (USA).

2.2. Methods

The fabrication and characterisation of the novel composite Z-pins testing was carried out in a number of steps. The first step was to process the individual PBO fibre tows into unidirectional or twisted tows, followed by pultrusion of these tows to form Z-pin rodstock. The rodstock was then introduced into an E-glass/913 epoxy laminate as single z-pins and tested at a range of different load mode mixities. The pultrusion and characterisation procedure was carried out as described in an earlier paper [26] and is detailed below.

2.2.1. Production of the Z-pin rodstock

The chosen manufacturing method to produce Z-pins was micro-pultrusion, and can be divided into the following steps:

- Two 273HM PBO fibre tows were twisted together using a micro-braiding machine. Each tow was then used individually to produce Z-pin rodstock.
 - a. An almost unidirectional fibre tow was produced by employing a large lay length of 500 mm.
 - b. A twisted tow was produced using a lay length of 2 mm. This corresponds to the distance between each twist of the tow.
- The dry PBO tows were fed through a series of rollers into a resin bath holding the blended monomers of either the bismaleimide triazine resin (BT) or the ductile epoxy resin (DCT). The tow was impregnated with the resin system and fed into a heated die. The

purpose of this die was to shape the uncured composite into a cylindrical rod by only achieving the gelling of the resin. The temperature of this die was of 100 °C for the DCT resin and 200 °C for the BT resin.

- Each pultrusion was carried out at a rate of 1 mm/s. The gelled rodstock was then placed into an oven to undergo a full curing cycle. Pins containing the BT resin were cured at 200 °C for 4 h. The DCT-based pins were cured for 2 h at 100 °C.

The characteristics of the fibres used, and the expected final properties of the resin systems used are given in Table 1 and Table 2, respectively. Fig. 1 shows the pins after pultrusion and prior to insertion. The dimensional characteristics of the pins are also summarised in Table 3, including the calculated average volume fraction (V_f) per pin. Note that the uPBO pins exhibited a more oval cross-sectional shape than the tPBO pins. This has been accounted for in the calculations and its impact will be discussed in the following sections.

2.2.2. Fabrication of test coupons

The chosen composite laminate manufacturing method for the host laminate was standard pre-impregnated layup of E-glass fibres within a Hexcel 913 epoxy resin system. It is an autoclave cured system with a curing temperature of 125 °C, which ensures that the DCT-based pins never reach their ultimate T_g (Table 1). A quasi-isotropic, anti-symmetric layup of [(0/45/90/-45)₃/0]_s//[(90/-45/0/45)₃/90]_s was employed. A thin PTFE release film was inserted at the 0/90 mid-plane (denoted by //). This layup was chosen to ensure that there was no nesting of the fibres across the film during cure.

The novel Z-pins were introduced across the full thickness of the uncured laminate by means of a direct insertion method as described by Lander et al. [32] and employed in previous research work [15,16,33,26]. Once the laminates had been cured in an autoclave oven, they were machined down into individual specimens. Each one included a single Z-pin at the centre of a 16 mm x 16 mm coupon with an average thickness of 8 mm, as depicted in Fig. 2.

2.3. Test procedure

The chosen method of characterisation for the novel Z-pins is single pin bridging tests using an Arcan rig. The rig was developed at the University of Bristol and employed to carry out pin bridging tests previously [16,17,26]. It allows the rotation of the coupon's midplane from 0° to 90° in 15° intervals. These angles correspond to the nominal interlaminar load mode mixity acting on the Z-pin as it bridges the top and bottom laminates, as seen in Table 4. The test rig was clamped to a Shimadzu AGS-X 1kN precision universal tester. The test rate used corresponded to a crosshead displacement of 1 mm/min. Tests were ended manually when the load dropped to zero (either after full pull-out

Table 1
Comparison of the mechanical properties of PBO fibre and carbon fibre.

Fibre	Tensile Modulus	Tensile Strength	Specific gravity	Filament Diameter	Elongation
<i>Units</i>	<i>GPa</i>	<i>GPa</i>	–	<i>µm</i>	<i>%</i>
PBO (HM Zylon) [28]	270.0	5.8	1.56	15.0	2.50
CF (T300) [29]	230.0	3.5	1.76	7.0	1.50

Table 2
Typical properties of the resin systems used in this study. ^a The mechanical properties of the BT resin are expected to lie within the boundaries of its constituent resin systems, hence that of cyanate esters and bismaleimides have been quoted [30].

Resin	Tg	Elongation	Flexural Modulus	Ultimate Strength
<i>Units</i>	<i>°C</i>	<i>%</i>	<i>GPa</i>	<i>MPa</i>
BT [30,31]	226–235	2.5–2.8 (CE) ^a 1.6–2.3 (BMI) ^a	2.7–5.9 (CE) ^a 3.6–4.8 (BMI) ^a	56–120 (CE) ^a 590 (BMI) ^a
DCT [27]	144–154	8–10	2.7–2.9	120–135

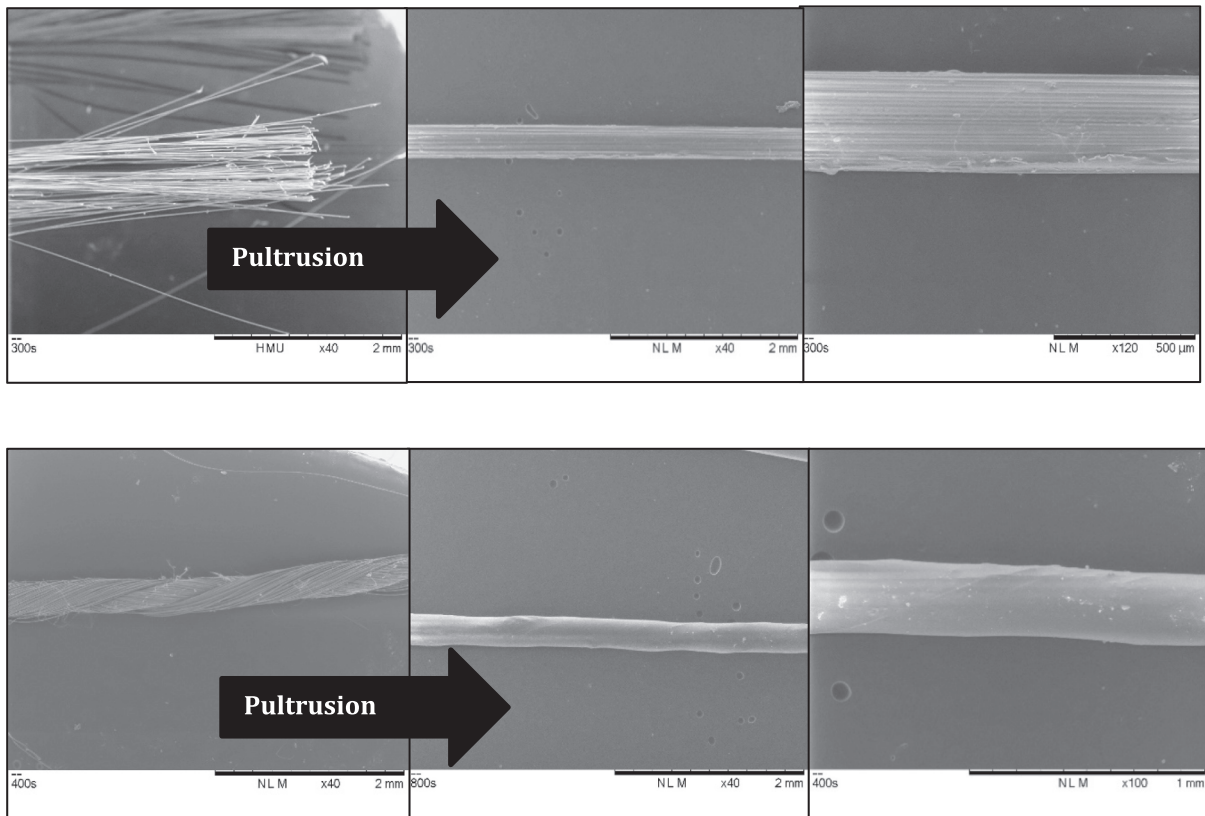


Fig. 1. SEM images of the unidirectional (top) and twisted (bottom) PBO fibres before and after the pultrusion process.

Table 3

Measured dimensions of the three types of Z-pins manufactured in this study, including the calculated fibre volume fraction (V_f). Note that the cross-sectional area for the uPBO pins was calculated as the area of an oval, measuring a short and long diameter per pin.

Pin Label	Fibre	Resin	Mean Diameter (μm)	Average Cross-sectional Area (mm^2)	V_f (%)
uPBO/DCT	Unidirectional PBO	DCT	290	0.0632	55.4
tPBO/DCT	Twisted PBO	DCT	270	0.0573	61.1
uPBO/BT	Unidirectional PBO	BT	280	0.0608	57.6

or rupture of the pin).

The Z-pin insertion procedure introduces some level of unavoidable misalignment. The true load mode mixity will differ from that generated

by the nominal angle of the Arcan rig and needs to be adjusted to reflect pin misalignment. The pin position in the top and bottom of the laminate was individually measured. The deviations in the x and y directions were used to assess pin misalignment. The misalignment values were used to calculate the adjusted load mode mixity (Φ) using Eq. (1). This method of assessing true load mode mixity is crucial to understand the behaviour of each individual pin and has been demonstrated in previous studies [16,26].

$$\phi = \sqrt{\cos^2\chi \sin^2\zeta + \sin^2\chi (\sin^2\psi + \cos^2\psi \cos^2\zeta) - \frac{1}{2} \sin 2\chi \sin 2\zeta \cos\psi} \quad (1)$$

Table 4

Corresponding load mode mixity for each nominal angle orientation of the Arcan rig.

Angle	Nominal load mode mixity (Φ)	% Mode I	% Mode II
0	0	100	0
15	0.26	74	26
30	0.50	50	50
45	0.71	29	71
60	0.87	13	87
75	0.97	3	97
90	1	0	100

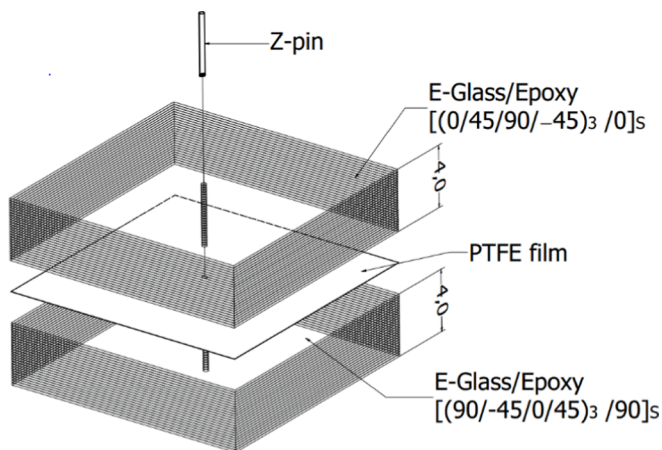


Fig. 2. Schematic representation of a single pin bridging coupon. Note that it is the exact same construction as used in a previous study [26].

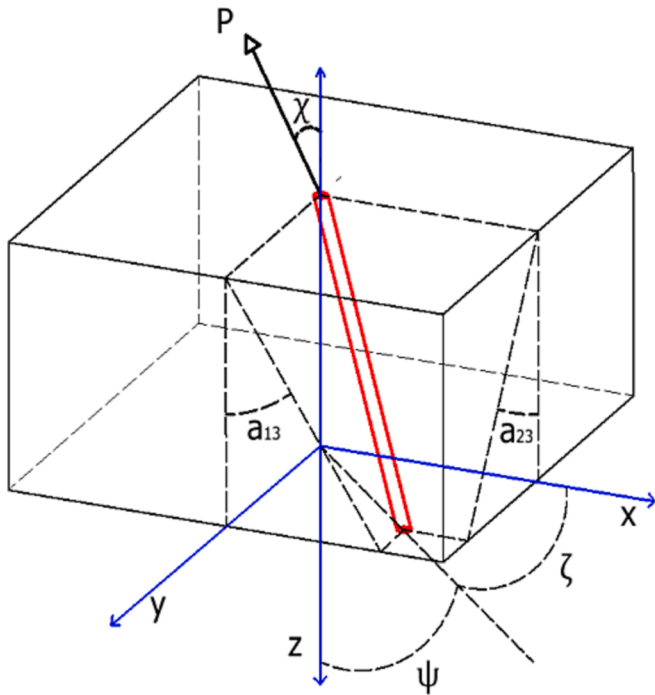


Fig. 3. Diagram illustrating pin misalignment and the conventions used to calculate the true mode-mixity with respect to the loading direction [26].

χ corresponds to the angle between the normal loading direction and pin insertion axis, the nominal rotation of the arcan rig. ψ and ζ are the off-set angles of the pin from the x-axis and the z-axis, respectively. These are all represented in Fig. 3. a_{13} and a_{23} had to be obtained trigonometrically and used in Eqs. (2) and (3):

$$\tan \zeta = \sqrt{\tan^2 a_{13} + \tan^2 a_{23}} \tag{2}$$

$$\tan \psi = \frac{\tan^2 a_{23}}{\tan^2 a_{13}} \tag{3}$$

The load displacement curves for each test coupon were evaluated to understand the difference in single pin bridging between the two novel Z-pins presented in this study. The area under the curve corresponds to the energy absorbed per pin during delamination. This energy value can be used to provide a measure of the apparent fracture toughness of the pinned laminate by employing Eq. (4):

$$G^*(\phi) = \frac{4\rho}{\pi D^2} \Psi(\phi) \tag{4}$$

where $\Psi(\phi)$ is the energy absorbed by a single pin during delamination, D is the diameter of the pin, and ρ is the pinning areal density (which is assumed to be 2% in this study).

For non-circular Z-pin cross-sections, Eqs. (4) and (5) can be substituted by 6 and 7 below, where A corresponds to the cross-sectional area of a single Z-pin.

$$G^*(\phi) = \frac{\rho}{A} \Psi(\phi) \tag{5}$$

$$\rho = \frac{A}{4W^2} \tag{6}$$

3. Results and discussion

The results from the single pin bridging tests are described and discussed in the following section. The effect of employing PBO-based Z-pins with different matrix systems and fibre architectures will be addressed. The behaviour of CF/BMI pins are used as a direct comparison. The microstructure of each pin is assessed, followed by the single pin bridging behaviour at mode mixities close to mode I, close to mode II and in the mixed-mode regime. The mode II section expands on data that has been previously presented at the 20th European Conference for Composite Materials [34]. All results are discussed and evaluated with the aid of scanning electron microscopy (SEM) of the failed coupons.

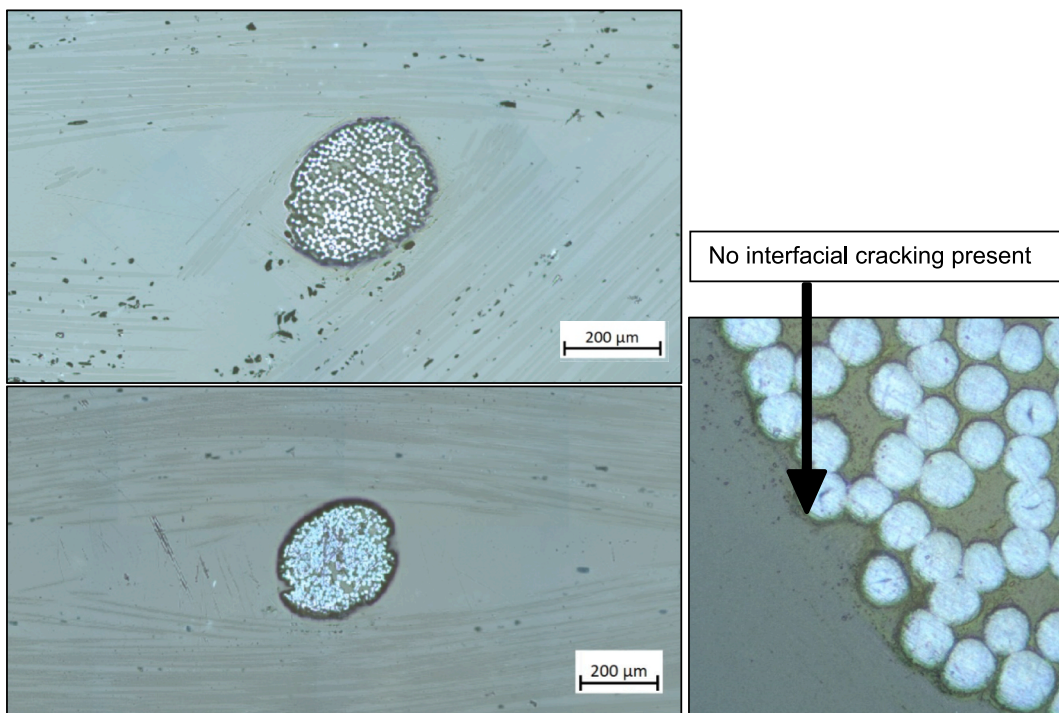


Fig. 4. Optical microscopy images of uPBO-based pins within an E-glass/Epoxy laminate. Notice that the dark halo is caused by the high toughness of the PBO fibre during polishing.

3.1. Unidirectional fibre pseudo-ductile Z-pins

3.1.1. Microstructure

The microstructure of the laminates embedded with uPBO showed typical features of Z-pin reinforced composites, as can be seen from the cross-sectional optical microscopy images in Fig. 4. There is bowing of the host laminate fibres around the pin, creating in-plane fibre waviness. The excluded volume created by the fibre waviness has resulted in the formation of resin pockets around the pin. Through-thickness fibre crimping is however minimal, a result of employing the direct insertion method of pinning [32] as opposed to the ultrasonic hammer [35]. Note that the dark halo around the pin in Fig. 4 is caused by the toughness of the fibre during the grinding and polishing process, and it is not due to void or crack presence. Further magnification as seen in the adjacent micrograph reveals that the interface is still largely present and crack-free.

There is a lower volume of appreciable interfacial void content and pre-cracking from what has been expected from earlier studies [7]. This correlates to the data presented in Section 3.1.3, and it can be a result of a less significant thermal mismatch between the cured pin material and the host laminate. Interfacial cracks between the pin and the laminate typically form during post-cure cool-down due to the inherent thermal mismatch between the cured composite rod and the cooling laminate. The latter has enveloped the pin during the cure cycle, yet as the temperature decreases, the mis-match in the temperature-induced shrinking promotes the formation of these interfacial cracks [36]. The laminate material has a moderately low temperature cure compared to typical aerospace-grade resin systems. The smaller temperature range during cool-down will reduce the effect of the thermal mismatch on pin-laminate residual interfacial stresses.

The overall quality of the pins manufactured in this study is comparable to that of commercially available pins. The cross-section of the pins themselves tends to be elliptical rather than circular. This has been taken into account when calculating the average cross-sectional area of the manufactured rodstock. However, the resulting asymmetric moment of inertia acting on the pin during bending may influence the variability of the data, and hence the data scatter.

3.1.2. Mode I bridging behaviour

Fig. 5 shows direct comparisons between representative load-displacement curves of uPBO/BT, uPBO/DCT and CF/BMI pins at a mode mixity below 10 % mode II ($\Phi = 0.1$). All curves show a pull-out failure mechanism, with elastic stretching, debonding and frictional

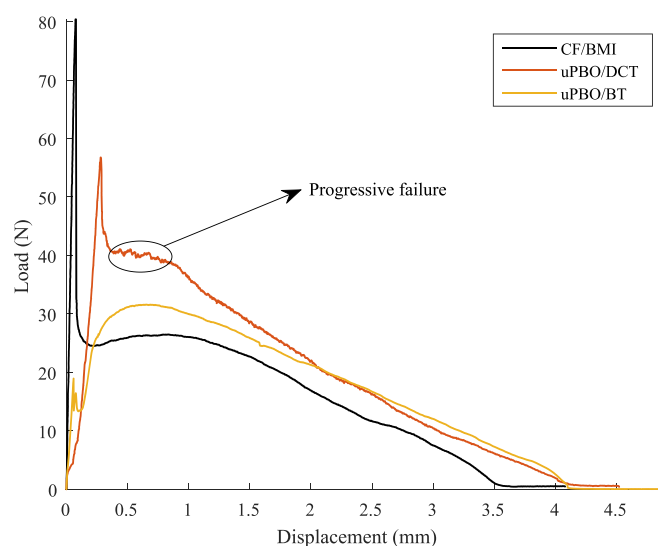


Fig. 5. Typical load displacement curves of coupons tested at a nominal angle of 0. Pins are subjected to primarily mode I loads.

pull-out stages [19]. However, the debonding peak force is significantly larger when CF/BMI pins are employed, suggesting that initial interface between the PBO-based pins and the laminate is weaker. Although Fig. 4 does not show any major interfacial debonding prior to testing, these are typically present to some extent. [7,37]. Regardless of different thermal mismatch values, all three pin types exhibit a peak load equivalent to the force needed to debond and commence pull-out, as seen in Fig. 5.

Both the uPBO/DCT and CF/BMI exhibit a peak debonding load followed by a large reduction in load and a stable pull-out. The traction load as it is pulled out decreases with crack opening displacement. The uPBO/DCT pin showed an around 25 % decrease from the debonding load to the initial pull-out traction load, but this decrease was much larger in the CF/BMI pin specimen. In comparison, the uPBO/BT pins exhibit a dramatically smaller debonding force, followed by a gradual increase in traction load, until the latter reaches a plateau. The uPBO/DCT sits at a mid-point between these two pins at the start of pull-out. The load necessary to begin pull-out is lower than that of the CF/BMI pins yet still almost three-fold that of the uPBO/BT; pull out also exhibits a stick and slip pattern. The latter is a consequence of the ductile surface of the pin, which is plastically deformed as the pin pulls out. The traction load remains stable as the surface of the pin is smoothly deformed above its shear yield strength, promoting a higher friction between the pin and laminate surfaces. The largest ductile deformation occurs just after the peak load and gradually decreases as the pin is pulled out, showing an almost linear reduction in traction force with displacement. In comparison, uPBO/BT pins easily debond from the laminate, due to the dissimilar BMI resin chemistry and CTE mismatch. The brittle surface of the pin can only rely on the residual interfacial friction to produce a traction force, which is not enhanced by surface ductility. The shape of the curve resembles that encountered by Yasae et al. [16,17], which is typical of a TTR rod with a more brittle resin. Once the pin debonds, the load necessary to pull the pin out gradually increases. This initial increase in friction can be attributed to matrix debris forced between the pin and the laminate as pull-out progresses, as seen in the work of Zhang et al. work [38]. As the pin is further pulled out, the load starts to decrease with reducing pin-laminate contact surface area. Ultimately, the energy dissipated through pinning is comparable for all the Z-pin types considered, as the final failure mode occurs because of complete pin pull-out.

The micro-graphs in Fig. 6 show how the pulled out uPBO/BT pin presents a relatively smooth, uniform surface. In comparison, the uPBO/DCT pin presents a rough, irregular surface marked by localised plastic deformation of the matrix. The dimpled and granular fracture surface is characteristic of a ductile failure [39]. It results in increased friction and overall energy dissipation. Debonding of the uPBO/BT pins occurs across a small shear displacement over. Brittle failure of the interface occurs swiftly; then the uPBO/BT pin begins to pull-out under friction. Comparatively, the DCT-based pins show a progressive drop in force. Interfacial and bulk matrix cracking progress along the length of the pin, followed pin pull-out. The latter promotes further plastic deformation of the matrix through friction. This requires a larger load and applied displacement. Additionally, it is possible that unreacted functional groups form the pin matrix could have formed a low-density network of crosslinks at the interface with the host laminate. Reactive functional groups have been previously demonstrated to promote pin-laminate bonding [25]. The resulting interfacial bonding would also explain the increased debonding force necessary.

3.1.3. Mode II bridging behaviour

As reported by Yasae et al. [16,17] and previous work by the authors of this paper [26], the bridging effectiveness of CF/BMI pins is dramatically lower under loading conditions close to mode II. The decrease in apparent interlaminar toughness and pin bridging performance has been previously linked to a failure mode transition [17]. As the loading mode mixity increases from mode I to mode II, the increasing shear acting on the pin is sufficient to promote fibre failure at stress

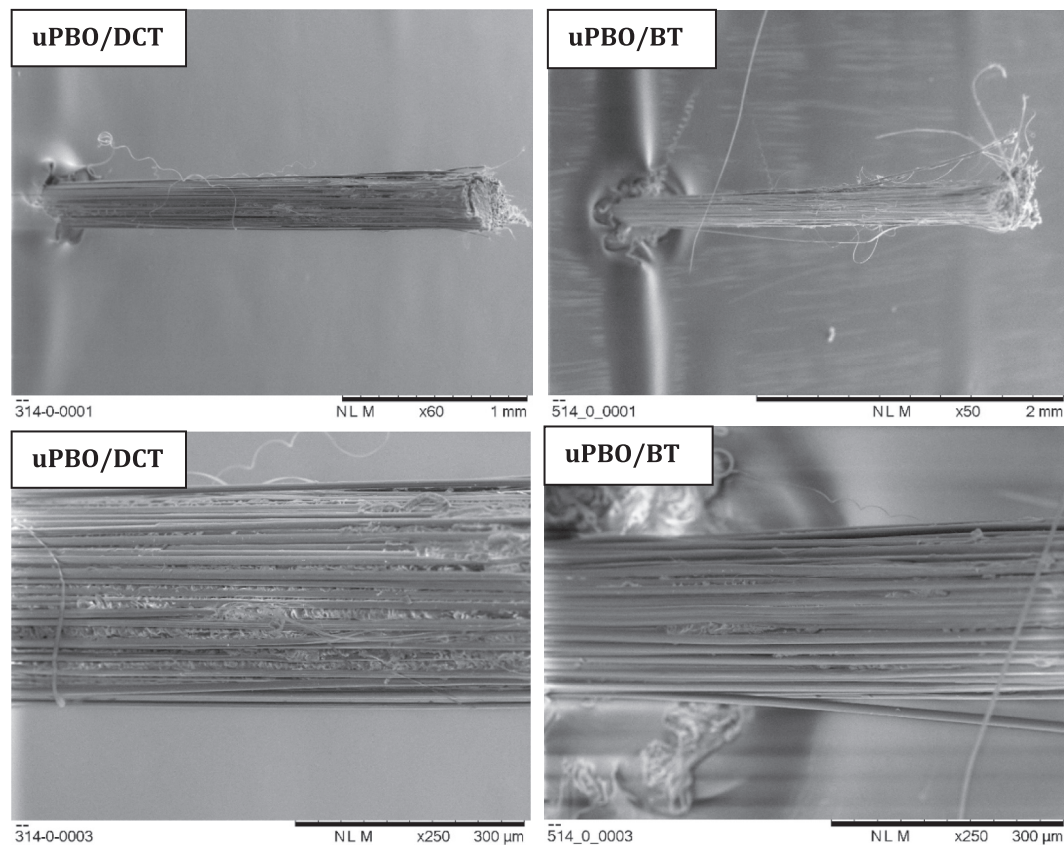


Fig. 6. SEM micrographs of the uPBO based pins after a successful pull-out test.

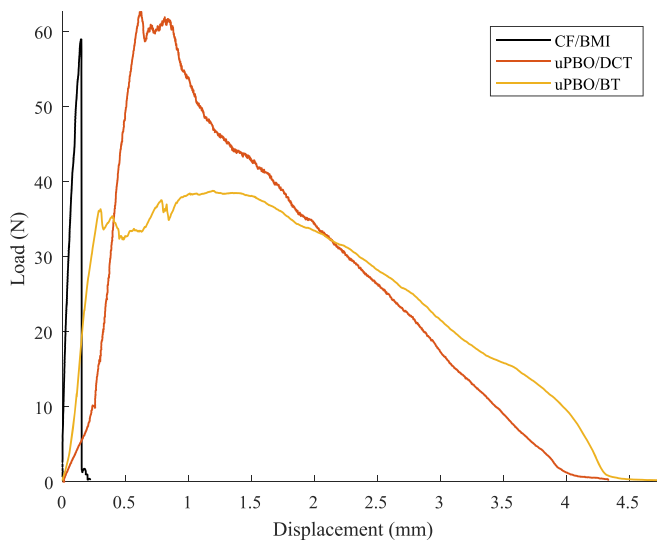


Fig. 7. Load displacement curves of unidirectional PBO-based pins at a mode mixity close to mode II (higher than 97 % mode II).

concentration regions. In comparison, the failure mechanism of the uPBO pins does not change during mode II delamination, as it still consists in complete pin pull-out. Fig. 7 shows the characteristic load displacement curves, including that of the CF/BMI pins. The curves of uPBO pins are similar in shape with those recorded at mode mixities closer to mode I. uPBO/DCT pins still show a notably larger debonding stage than uPBO/BT, as well as the characteristic stick/slip response thereafter. Even at mode mixities as high as 97 % mode II, the pins can completely pull out under the increased shear load.

The ability of both pin types to keep pulling out under high mode II loads is a key novel behaviour. It is typical of metallic Z-pins due to their ductility [10,11], but it has not been previously reported for fibrous composite Z-pins. Additionally, as seen by the mode I results, the traction loads exhibited at lower mode mixities are superior to that of standard, untreated metallic pins [10]. This is a crucial difference when comparing both pin types. Surface treatment may improve metallic pin performance by increasing interfacial adhesion and friction [13], yet it does not address the galvanic corrosion issues of including a metal pin within a composite laminate. The SEM images in Fig. 8 are a good indication of the failure mechanism of the PBO-based pins and its difference from traditional CF/BMI pins. At mode mixities above 97 % mode II, uPBO/BT and uPBO/DCT have both pulled out fully and exhibit permanent deformation along the delamination plane. There is no visible fibre failure, but there is extensive matrix failure. Substantial longitudinal crack formation separates each Z-pin into smaller fibrils and fibre bundles, increasing their ability to bend under the shear load. The fibres can extend and bend past the shear strain to failure of the matrix system without fibre failure. This is an occurrence that has been reported previously for CF/BMI pins at lower mode mixities [26]. Under mode II dominated loads however, CF-based pins rupture with negligible pull-out as seen in the load displacement curve in Fig. 7. The bending and dramatic fibrillation of the pins is brought about by the combined high strength and toughness of the PBO fibres. In particular, the elongation at break of 2.5 % compared to 1.5 % of CF ensures that the initial bending necessary to promote pull-out does not result in fibre failure. The bending of the pin under shear helps to transfer the load along the TTR axis, *i.e.* along the fibre direction. The 5.5 GPa tensile strength of the PBO fibres ensure that the axial load is not sufficient to cause tensile failure. The combination of these material properties therefore promotes the pull-out of the pin regardless of the mode-mixity during delamination bridging. The resulting force required to complete

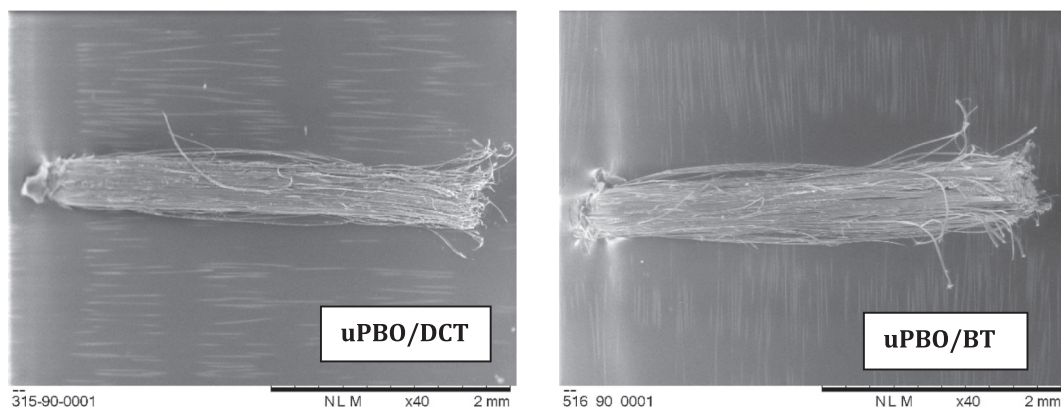


Fig. 8. SEM micrographs of the uPBO based pins after a successful close to mode II bridging test.

the pull-out failure translates into a higher energy dissipation than when brittle CF-based pins are employed. Ultimately, the matrix choice has a second order effect on the pin behaviour.

Furthermore, the pseudo-ductile behaviour may not be limited to PBO-based Z-pins. As long as the fibre choice has the correct minimum strength and elongation, the fibres should be able to withstand the bending deformation, promoting longitudinal matrix failure and pull-out. However, these threshold properties will be dependent on loading conditions as well as the characteristics of the host laminate. Correctly defining and modelling the failure mechanisms observed in composite Z-pins under large bending deflections is essential to determine these thresholds, and forms part of the necessary follow-up work for this study. Likewise, alternative characteristics such as the matrix properties and the fibre–matrix interface could as well be engineered to fail at low loads and achieve a similar effect, as seen in [26].

The difference in filament diameter between CF and PBO (7 μm and 12 μm), may also influence the shear strength of the individual filaments

and contribute to the effectiveness of the larger PBO, particularly at preventing premature failure of the pin before debonding. However, in most cases, fibre failure occurs under bending-induced tension at the delamination plane [17,40]. Evidence of tensile failure of the PBO filaments is further seen in Section 3.2.

3.1.4. Single pin bridging behaviour across full mode mixity range

As can be seen from Fig. 9, both pins reinforced with longitudinal PBO fibre, uPBO/DCT and uPBO/BT, exhibit an apparent toughness that gradually increases with the mode-mixity. The shaded areas on Fig. 9 represent the scatter of data, given by a single standard deviation above and below the best-fit average line. The uPBO/DCT pins show the largest variability. In terms of minimum expected energy absorbed per pin, both TTR types yield similar results. However, the maximum energy dissipated is 8 % higher for the uPBO/DCT pins at mode mixity values close to Mode II ($\Phi = 1$). The apparent toughness of CF/BMI pins, is also shown for direct comparison. Up to a mode mixity of 0.2, all three pin

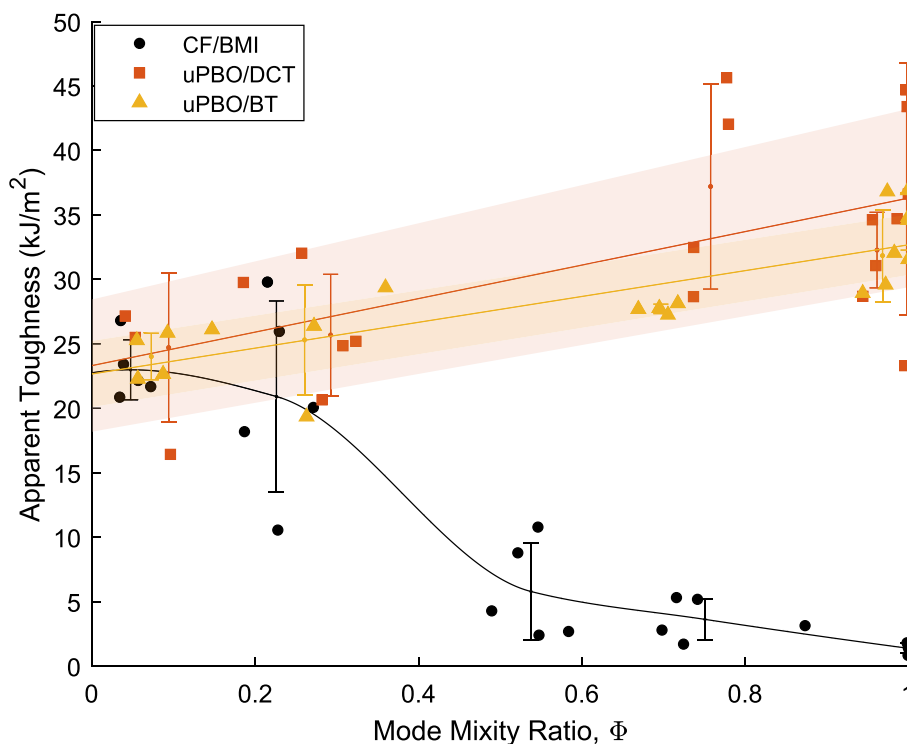


Fig. 9. Apparent delamination toughness derived from single pin bridging tests at different mode mixity ratios, accounting for pin misalignment and assuming 2 % pinning areal density. The shaded regions correspond to the best fit average maximum and minimum energies. The shaded regions correspond a single standard deviation above and below the best fit average energy.

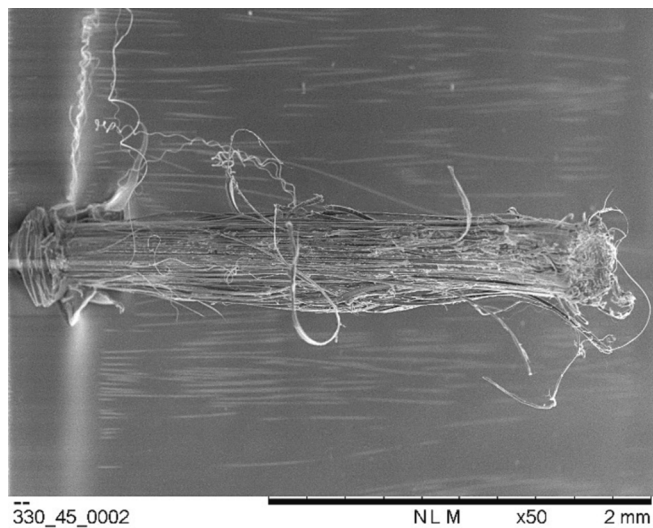


Fig. 10. SEM image of a uPBO/DCT pin after being pulled out at a nominal load mode mixity of 0.71. Notice the extensive matrix damage and permanent deformation.

types behave similarly. Above 0.2, the energy absorbed by the CF-reinforced pins starts to decrease. In comparison, the dissipated-energy trend for both PBO-based pins increases up to an average of 32–35 kJ/m² in a mode II regime. The key difference between the behaviour of the PBO-based pins and the CF-based pins is down to the pin failure mode. Above 20 % mode II, carbon fibre pins enter what has been previously identified as a pull-out to rupture transition region [16,17,26]. Beyond this region, the pins fail by fibre rupture, after little to no pull-out. The energy dissipated by this process is dramatically lower and results in poor mode II toughness enhanced when compared to mode I performance. As can be seen in Fig. 10 and the representative load–displacement curves in Fig. 11, as the proportion of mode mixity

increases, the uPBO pins still undergo pull-out. The load carried across a wide displacement range corresponds to a large energy dissipation value.

Increasing the loading mode mixity of the uPBO pin changes the peak force value in the load–displacement curve. As seen in Fig. 10, the peak tends to move towards a higher displacement, *i.e.* it occurs further into the pull-out process. This effect is the result of the faster damage progression within the pin during pull-out, and an increased frictional load at higher mode mixities. For the pin to be pulled out at higher mode mixities, it has to undergo extensive matrix failure and deform further prior to as well as during pull-out. Evidence of this can be seen in the micrographs in Fig. 10.

The superior performance of uPBO over the traditional CF/BMI Z-pins has been made clear through these results. The apparent interlaminar fracture toughness values shown are a direct measure of the ability of a single pin to bridge an interlaminar crack, at its wake. These values will differ from the true apparent interlaminar fracture toughness values obtained from standardised tests, where there is energy expenditure in fracturing the laminate itself. However, as established in the literature [7,10], most of the interlaminar fracture toughness enhancement by Z-pinning occurs through crack-bridging during the propagation of a delamination. Therefore, it is expected that the difference in effectiveness between Z-pin types will translate to larger scale tests, as long as these allow sufficient crack opening and sliding displacements. Nevertheless, these larger scale tests will be a necessary next step to fully understand the hierarchical behaviour of novel pseudo-ductile Z-pinned laminates.

3.2. Twisted fibre pseudo-ductile Z-pins

3.2.1. Microstructure

The microstructures of the laminates pinned with the twisted PBO pins (tPBO) resemble that seen both for the uPBO-based pins and what has been previously reported for carbon-fibre Z-pins [41–43]. Fibre waviness and resin pockets are of comparable size and geometry to those presented in Section 3.1.1. Perhaps the most notable difference is the

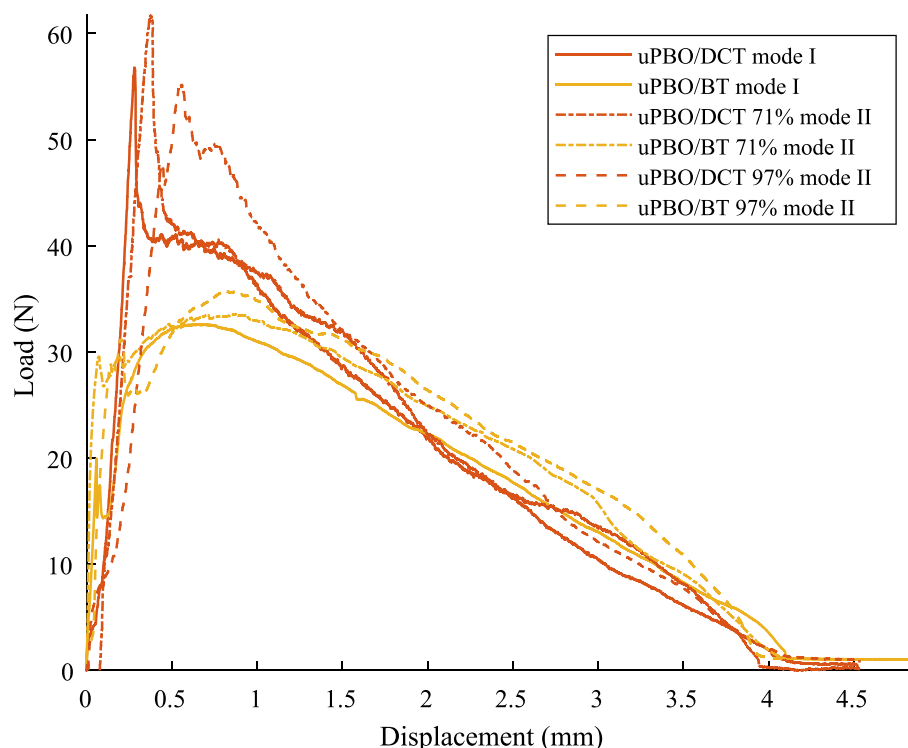


Fig. 11. Typical load–displacement curves of uPBO-based pins at a range of different mode mixities. Notice the minimal change with proportion of Mode II load.

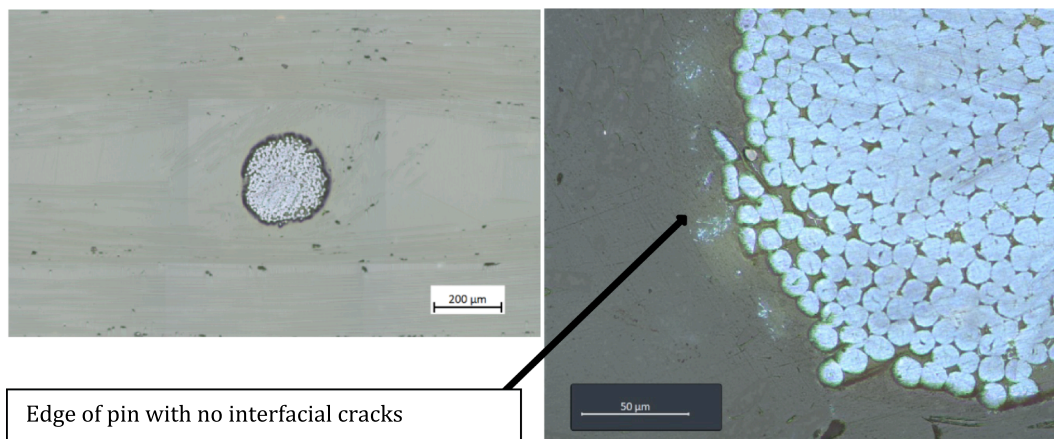


Fig. 12. Optical microscopy image of two tPBO/DCT pins embedded in an E-glass laminate.

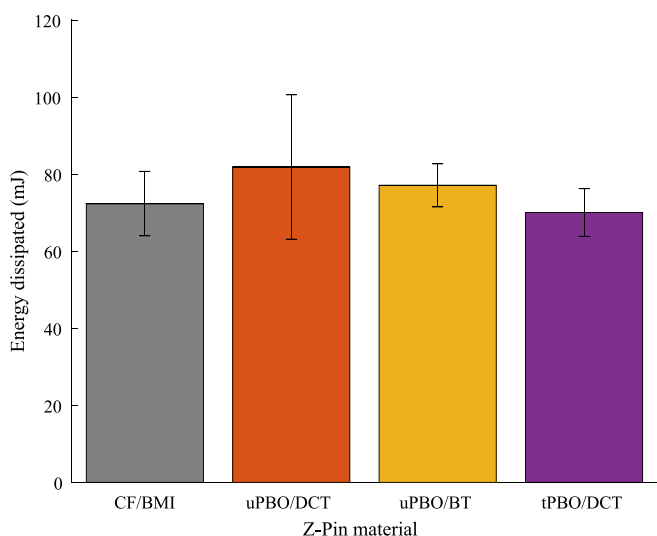


Fig. 13. Average energy dissipated per pin at mode mixities below 10 % mode II.

structure of the Z-pin itself. As can be seen from the cross-sectional image in Fig. 12, the effect of twisting the fibres promotes the formation of an almost circular cross-section, different from the elliptical one observed in the uPBO pins. The twist itself tends to cluster the individual filaments together, creating a packed fibre architecture. One can observe that there is a central fibre bundle that remains relatively circular whilst the second bundle wraps around it completely. Both bundles contain the same number of filaments. The result is a pin with a smooth surface and a higher degree of fibre compaction. However, most of the resin matrix tends to migrate towards the outer part of the Z-pin.

3.2.2. Mode I bridging behaviour

Fig. 13 summarises the energy dissipated per pin under a load mode mixity lower than 0.1. At this point, the effectiveness of tPBO pins can be directly compared with that of the uPBO pins and with that of typical CF-based pins. All pins have comparable energy dissipation, with overlapping data scatter values. Nonetheless, uPBO/DCT pins show the best average performance. The lowest data variability between DCT-based candidates is seen in the tPBO/DCT pins. This can be explained by the improved geometrical quality of the twisted PBO Z-pins. As explained in section 3.2.1, twisting the PBO fibres at small lay lengths (*i.e.* under 5 mm) increases the geometric stability of the tow. Ultimately, this results in consistently circular and uniform-diameter rodstock cross-section. The variability in the delamination bridging action is thus reduced.

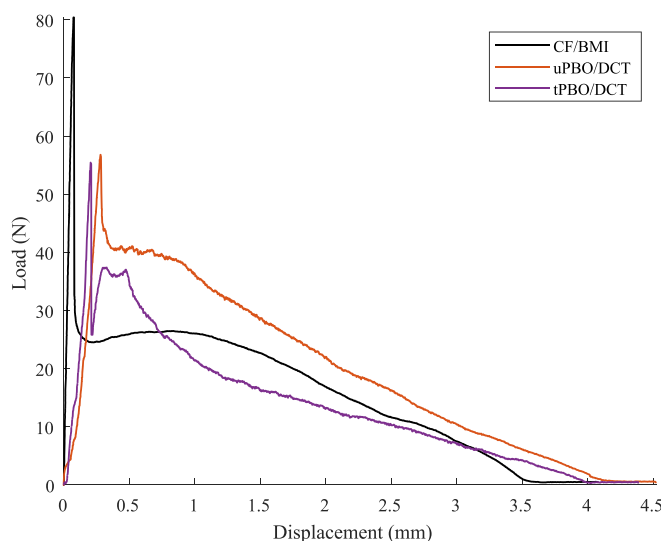


Fig. 14. Typical load displacement curves comparing the effect of fibre architecture on the delamination bridging performance at mode mixities below 0. 1.

Interestingly, even though the overall bridging energy dissipated is comparable, the load–displacement curves show different bridging mechanisms among all the three types of Z-pins considered (see Fig. 14). Whilst, the CF/BMI pins are characterised by a large debonding force followed by a comparatively weak pull-out traction force, the tPBO pins behave similar to the uPBO/DCT. The debonding force is lower, at an average of around 50 N per pin, followed by the characteristic progressive pull-out failure, as discussed in Section 3.1.2. Although both pin types employed the same matrix system, the region of progressive matrix failure is significantly narrower for the tPBO/DCT samples than in the uPBO/DCT. This is due to the smoother surface of the tPBO/DCT pins, which reduces the initial residual friction and mechanical interlocking during pull-out. The overall lower performance of the tPBO pins under mode I loading can be attributed to their microstructure as explained in Section 3.2.1. Twisting has promoted a smooth, uniform fibre surface which can reduce the mode I traction loads.

3.2.3. Mode II bridging behaviour

The area of greatest difference in the pin bridging behaviour of the tPBO pins is at loading mode mixities close to mode II. The overall energy dissipation chart in Fig. 15 and the load displacement curves in Fig. 16 represent these single pin bridging tests, (larger than 90 % mode II). At this mode mixity, the twisted PBO pins are within the pull-out to

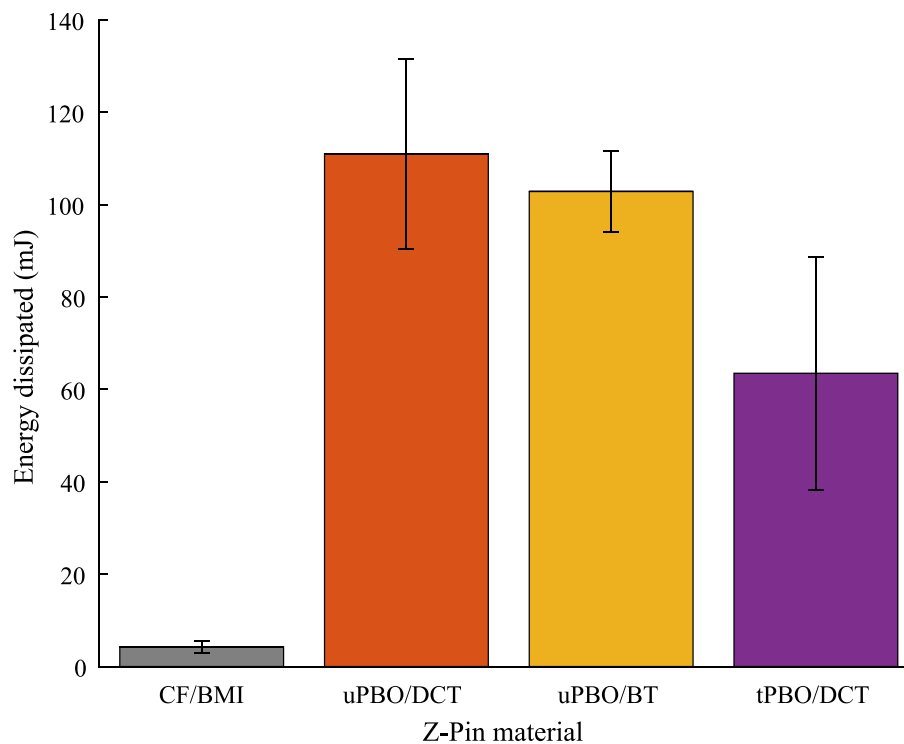


Fig. 15. Bar chart showing the average energy dissipated per pin at load mode mixities above 90 % mode II. The graph contains the three types of pseudo-ductile pins fabricated in this study. The energy dissipation value for CF/BMI is given as a direct comparison.

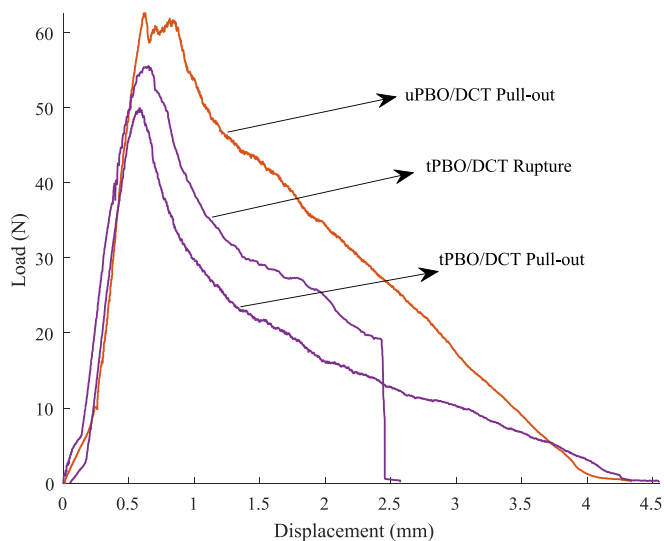


Fig. 16. Representative load displacement curves of uPBO/DCT and tPBO/DCT pins tested at mode mixities of around 97 % mode II. Pin rupture and pin pull-out curves have both been included for the tPBO pin type.

rupture transition, which occurs at a 20 % mode II in CF/BMI pins [26]. Whilst the dissipated energy is significantly larger than that of the typical CF/BMI pins, which rupture under these conditions, on average tPBO pins dissipate 40–45 % less energy per pin than the uPBO/DCT and the uPBO/BT. However, this is still a 10-fold increase in comparison to the energy dissipated by the CF/BMI pins [26]. The tPBO pins also exhibit a larger data variability. A number of tPBO pins ruptured at mode mixities above 90 % mode II, however, others were fully pulled out at a mode mixity above 97 % mode II.

From the load displacement curves and the micrographs in Fig. 17, two distinct characteristics can be linked to the lower bridging

performance. The first feature is the inability of tPBO to consistently pull out under shear dominated loads. A pin that ruptures prior to full pull-out will dissipate significantly lower energy. The second feature is the load carried by the pin during pull-out. This is smaller on average than that of the uPBO samples. The latter is a direct effect of the smoother surface and smaller diameter of the twisted pin, as seen in the mode I case. The smoother pin surface and reduced surface area has a detrimental effect on friction. The reduced friction enables pin pull-out at lower traction loads, which translates into reduced energy dissipation.

The second feature of the twisted fibre architecture is the reduced ability of the pin to separate into fibre bundles. As evidenced from the micrographs in Fig. 17, some fibre separation occurs, yet it tends to be only between the two twisted filament bundles instead of the extensive fibrillation seen in the uPBO/DCT samples (Fig. 8). This results in two large overlapping fibre bundles compressed against each other. Eventually, the stress concentration building at the fibre overlap location results in PBO fibre failure. The position of these overlapping fibre bundles may affect the possibility of fibre failure in twisted pins. As the pin is pulled out, the region of concentrated stress due to fibre overlap will eventually align with the region of highest tensile stress at the delamination plane. However, this may occur later in the pull-out process, when the traction load has decreased enough to prevent fibre failure. This mechanism can explain the variability in failure modes observed for the tPBO pins.

3.2.4. Single pin bridging behaviour across full mode mixity range

The overall effect of employing pseudo-ductile Z-pins with a twisted fibre architecture is presented in Fig. 18, which compares the apparent toughness of the tPBO/DCT with that of the uPBO/DCT pins. As already done in Sect. 3.1.4, the behaviour of CF/BMI pins is shown for direct comparison. Data variability for the tPBO pins is significantly narrower than that of the uPBO pins close to mode I. The scatter in performance of the tPBO pins increases as the mode mixity ratio approaches mode II. Fig. 19 shows the data scatter observed among the samples in terms of their individual load–displacement behaviour. At mode mixities below

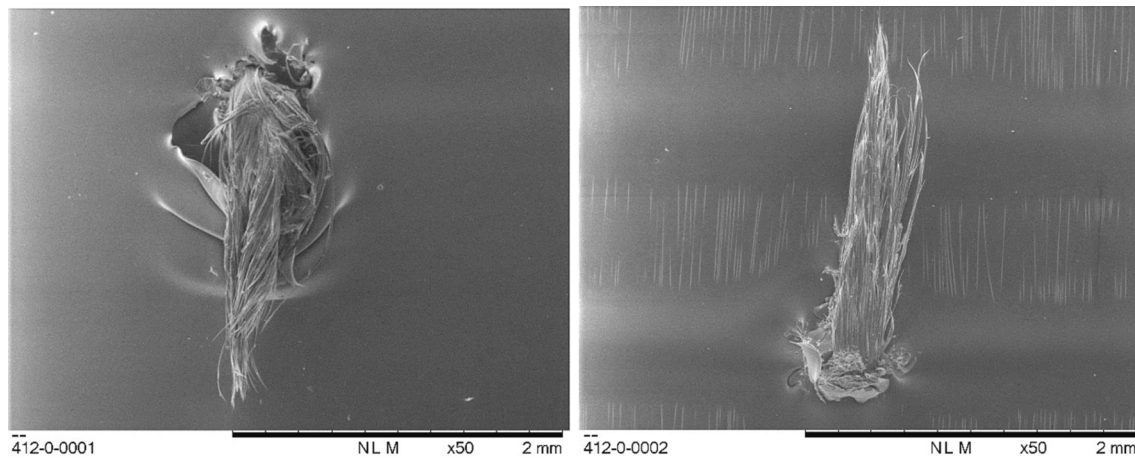


Fig. 17. SEM images of a tPBO pin ruptured during a high mode II single pin bridging test. It exhibits large plastic deformation and extensive matrix and fibre failure.

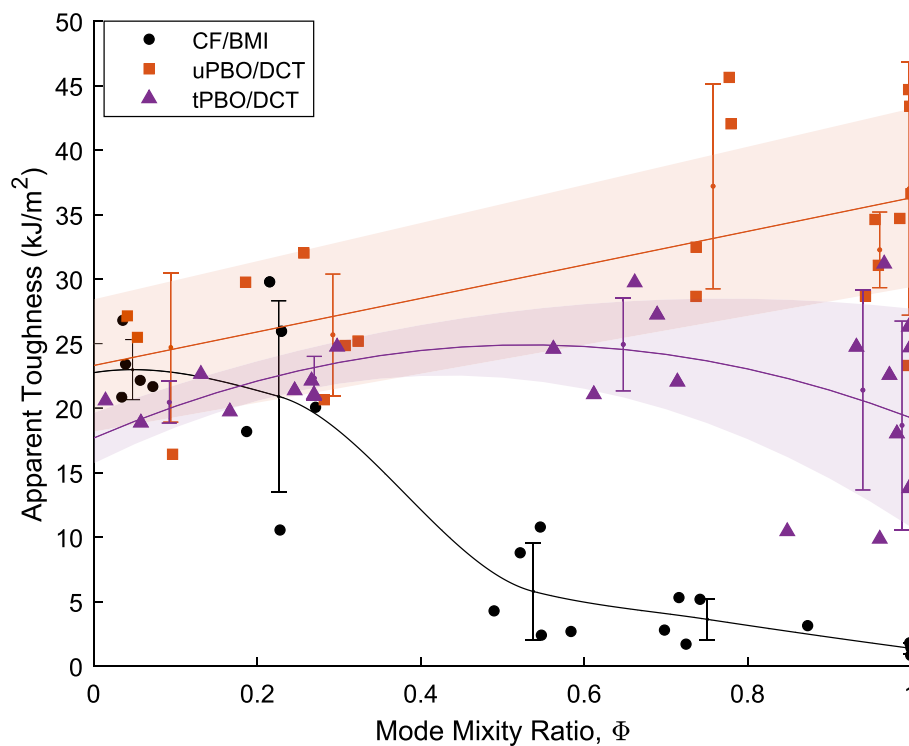


Fig. 18. Apparent delamination toughness of derived from single pin bridging tests at different mode mixity ratios, accounting for pin misalignment. The shaded regions correspond a single standard deviation above and below the best fit average energy.

0.2, it is evident that the pin behaviour of the tPBO pins is similar to that of CF and uPBO. As with the unidirectional PBO fibres, the energy absorbed by the tPBO pins increases with increasing mode mixity. This occurs up to a mode mixity of 70 % mode II, beyond which the average energy absorbed per tPBO pin tends to decrease. There is a particularly dramatic drop in pin performance above 0.9 mode mixity, which corresponds with the pull out to rupture transition discussed in the previous section. The increase in variability of the data gathered as the load mode mixity increases can be traced back to a more complex failure mechanism as the proportion of mode II load increases. As with the uPBO/DCT pins there is extensive matrix cracking, albeit this is more localised in the region between the two twisted fibre bundles. Evidence of this is seen in Fig. 20, which shows how at mode mixities of 0.7, the tPBO pins tend to unravel and separate into two individual bundles. This is sufficient to promote pull-out at high mode mixities, yet it is not as ductile a

mechanism as the full pin fibrillation observed in the uPBO-based pins. Adding to the discussion made in Section 3.1, as with the uPBO samples, the behaviour observed is primarily due to the high tensile strength and elongation at break of the fibres. It may be possible that this behaviour is not unique to PBO-based Z-pins, nevertheless, a combination of a high tensile strength and strain to failure is essential.

4. Conclusions

The effect of fibre properties on the bridging performance of Z-pins has been studied in this paper. It has been achieved through the manufacture and characterisation of novel pseudo-ductile fibrous composite Z-pins based on PBO fibres. There are several conclusions to be drawn from the results:

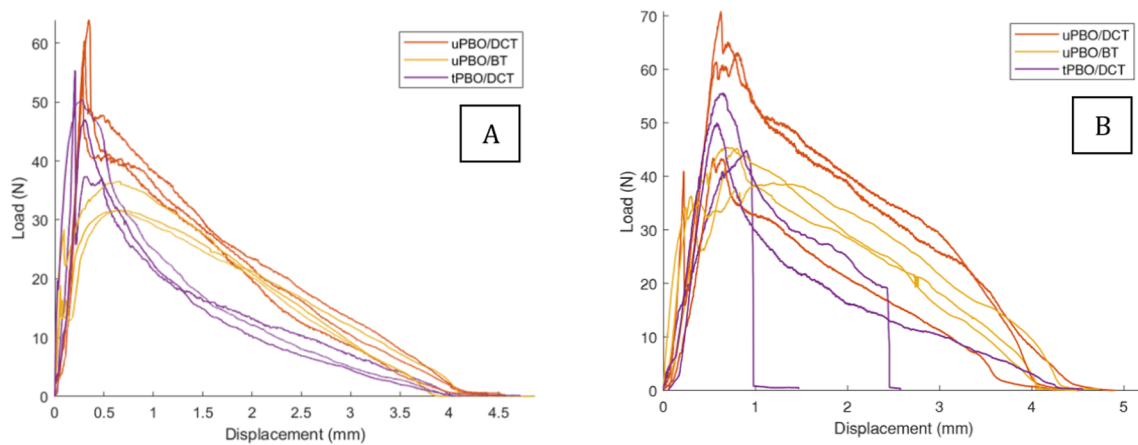


Fig. 19. Load-displacement graphs showing the data variability among samples tested under mode I (A) and mode II (B).

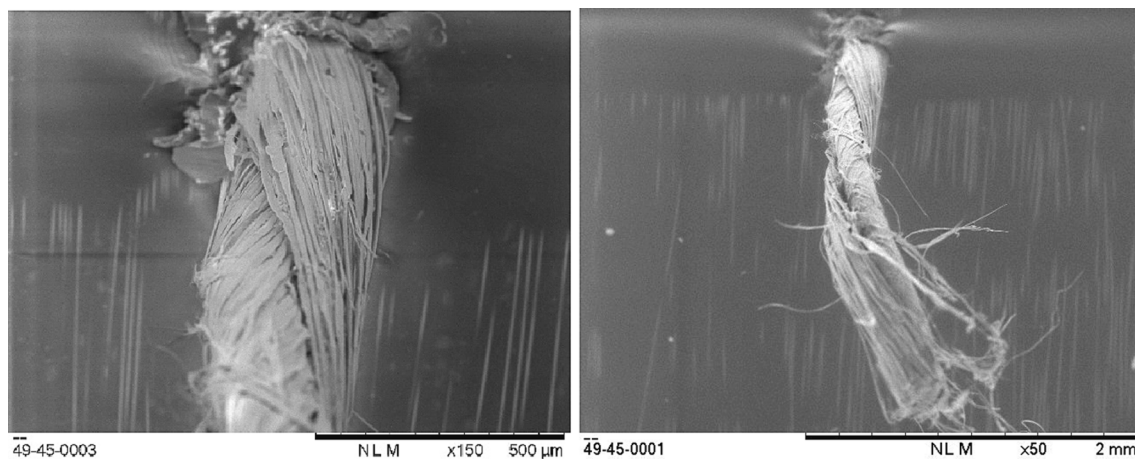


Fig. 20. Scanning electron microscopy images of tPBO/DCT pulled out of the host laminate at a mode mixity of 0.71.

- 1) The most effective way of improving the interlaminar toughening of Z-pinned composites is to achieve Z-pin pull-out across the full mode-mixity range. The use of a high strength and elongation-to-failure fibres increases the damage tolerance of Z-pins, to the extent of enabling pull out in mode II dominated regimes. In these conditions, the matrix system fails under longitudinal shear and the pin separates into fibre bundles. This characteristic pin fibrillation ensures that pull-out can occur by allowing large bending deflections and transferring load along the Z-pin fibre direction. The traction load during pull-out remains high due to the inherent surface roughness of the composite material after the Z-pin/laminate interfacial failure.
- 2) The effect of the matrix mechanical properties yields a secondary effect if compared to those of the fibres. The use of a ductile matrix increases the energy dissipated per pin by an average of 2–8 % when compared to a brittle resin system throughout the full mode mixity range. However, the failure mechanism is not significantly altered, and pull-out occurs regardless of matrix choice. The ductile response of the matrix during pull-out promotes further energy dissipation, as the matrix must deform extensively prior to failing. The mechanism also increases the interfacial roughness during pull-out, resulting in a higher average traction force. Nevertheless, the failure mechanism results in higher statistical variability between tests, which makes the performance less predictable.
- 3) Twisting of two PBO fibre tows at small lay lengths (2 mm) promotes the geometrical stability of the pins during manufacturing, enabling the achievement of uniform circular cross sections. However, it has a detrimental effect on the pin behaviour during pull-out. The stress

concentrations created at the overlapping surfaces between the two distinct fibre bundles promote fibre failure at mode mixities above 90 % mode II. Furthermore, fibre compaction during pultrusion results in smaller pin diameter with higher effective volume fraction that is also smoother than unidirectional PBO pins. These factors result in a smaller traction loads during pull-out.

CRediT authorship contribution statement

E. Santana de Vega: Writing – original draft, Methodology, Investigation, Formal analysis, Data curation, Conceptualization. **G. Allegrì:** Writing – review & editing, Project administration, Funding acquisition, Conceptualization. **B. Zhang:** Writing – review & editing, Supervision, Methodology. **I. Hamerton:** Writing – review & editing, Supervision, Resources. **S.R. Hallett:** Writing – review & editing, Supervision, Resources, Funding acquisition, Conceptualization.

Declaration of competing interest

The authors declare that they have no known competing financial interests or personal relationships that could have appeared to influence the work reported in this paper.

Data availability

Data will be made available on request.

Acknowledgements

The authors wish to acknowledge the support of Rolls-Royce plc through the Composites University Technology Centre (UTC) at the University of Bristol and the EPSRC through the ACCIS Centre for Doctoral Training grant, no. EP/G036772/1.

References

- [1] Velmurugan R, Solaimurugan S. Improvements in Mode I interlaminar fracture toughness and in-plane mechanical properties of stitched glass/polyester composites. *Compos Sci Technol* 2007;67:61–9. <https://doi.org/10.1016/j.compscitech.2006.03.032>.
- [2] Dell'Anno G, Treiber JWG, Partridge IK. Manufacturing of composite parts reinforced through-thickness by tufting. *Robot Comput Integr Manuf* 2016;37:262–72. <https://doi.org/10.1016/j.rcim.2015.04.004>.
- [3] Wambua PM, Anandjiwala R. A review of preforms for the composites industry. *J Ind Text* 2011;40:310–33. <https://doi.org/10.1177/1528083709092014>.
- [4] Huang SL, Richey RJ, Deska EW. Cross reinforcement in a GR/EP laminate. *Am Soc Mech Eng Winter Annu Meet San Fr Calif* 1978:1978.
- [5] Krasnov VI, Kuznetsov VA, Maksakov AY. Automated method of transverse reinforcement of composites by short fibers. *Mech Compos Mater* 1987;23:356–61. <https://doi.org/10.1007/BF00811696>.
- [6] Tomashevskii VT, Shalygin VN, Romanov DA, Sitnikov SY. Transversal reinforcement of composite materials using ultrasonic vibrations. *Mech Compos Mater* 1988;23:769–72. <https://doi.org/10.1007/BF00616801>.
- [7] Mouritz AP. Review of z-pinned composite laminates. *Compos Part A Appl Sci Manuf* 2007;38:2383–97. <https://doi.org/10.1016/j.compositesa.2007.08.016>.
- [8] Kostopoulos V, Sarantinos N, Tsantalis S. Review of through-the-thickness reinforced z-pinned composites. *J Compos Sci* 2020;4:31. <https://doi.org/10.3390/jcs4010031>.
- [9] Mouritz AP. Review of z-pinned laminates and sandwich composites. *Compos Part A Appl Sci Manuf* 2020;139:106128. <https://doi.org/10.1016/j.compositesa.2020.106128>.
- [10] Cartié DDR, Cox BN, Fleck NA. Mechanisms of crack bridging by composite and metallic rods. *Compos Part A Appl Sci Manuf* 2004;35:1325–36. <https://doi.org/10.1016/j.compositesa.2004.03.006>.
- [11] M'membe B, Yasae M, Hallett SR, Partridge IK. Effective use of metallic Z-pins for composites' through-thickness reinforcement. *Compos Sci Technol* 2019;175:77–84. <https://doi.org/10.1016/j.compscitech.2019.02.024>.
- [12] Ju H, Nguyen KH, Chae SS, Kweon JH. Delamination strength of composite curved beams reinforced by grooved stainless-steel Z-pins. *Compos Struct* 2017;180:497–506. <https://doi.org/10.1016/j.compstruct.2017.08.018>.
- [13] Pingkarawat K, Mouritz AP. Comparative study of metal and composite z-pins for delamination fracture and fatigue strengthening of composites. *Eng Fract Mech* 2016;154:180–90. <https://doi.org/10.1016/j.engfracmech.2016.01.003>.
- [14] Cartié DDR, Troulis M, Partridge IK. Delamination of Z-pinned carbon fibre reinforced laminates. *Compos Sci Technol* 2006;66:855–61. <https://doi.org/10.1016/j.compscitech.2004.12.018>.
- [15] M'membe B, Gannon S, Yasae M, Hallett SR, Partridge IK. Mode II delamination resistance of composites reinforced with inclined Z-pins. *Mater Des* 2016;94:565–72. <https://doi.org/10.1016/j.matdes.2016.01.051>.
- [16] Yasae M, Lander JK, Allegri G, Hallett SR. Experimental characterisation of mixed mode traction-displacement relationships for a single carbon composite Z-pin. *Compos Sci Technol* 2014;94:123–31. <https://doi.org/10.1016/j.compscitech.2014.02.001>.
- [17] Allegri G, Yasae M, Partridge IK, Hallett SR. A novel model of delamination bridging via Z-pins in composite laminates. *Int J Solids Struct* 2014;51:3314–32. <https://doi.org/10.1016/j.ijsolstr.2014.05.017>.
- [18] Pingkarawat K, Mouritz AP. Improving the mode I delamination fatigue resistance of composites using z-pins. *Compos Sci Technol* 2014;92:70–6. <https://doi.org/10.1016/j.compscitech.2013.12.009>.
- [19] Pegorin F, Pingkarawat K, Daynes S, Mouritz AP. Influence of z-pin length on the delamination fracture toughness and fatigue resistance of pinned composites. *Compos Part B Eng* 2015;78:298–307. <https://doi.org/10.1016/j.compositesb.2015.03.093>.
- [20] Knaupp M, Scharr G. Manufacturing process and performance of dry carbon fabrics reinforced with rectangular and circular z-pins. *J Compos Mater* 2014;48:2163–72. <https://doi.org/10.1177/0021998313495070>.
- [21] Knaupp M, Baudach F, Franck J, Scharr G. Impact and post-impact properties of cfrp laminates reinforced with rectangular z-pins. *Compos Sci Technol* 2013;87:218–23. <https://doi.org/10.1016/j.compscitech.2013.08.018>.
- [22] Hoffmann J, Scharr G. Compression properties of composite laminates reinforced with rectangular z-pins. *Compos Sci Technol* 2018;167:463–9. <https://doi.org/10.1016/j.compscitech.2018.08.042>.
- [23] Hoffmann J, Sabban J, Scharr G. Pullout performance of circumferentially notched z-pins in carbon fiber reinforced laminates. *Compos Part A Appl Sci Manuf* 2018;110:197–202. <https://doi.org/10.1016/j.compositesa.2018.05.002>.
- [24] Wang XX, Chen L, Jiao YN, Li JL. Preparation of carbon fiber powder-coated Z-pins and experimental study on the mode I delamination toughening properties. *Polym Compos* 2016;37:3508–15. <https://doi.org/10.1002/pc.23550>.
- [25] Knopp A, Scharr G. X-ray photo-electron spectroscopic studies of cryogenic and plasma surface-treated z-pins. *J Compos Mater* 2017;51:1155–66. <https://doi.org/10.1177/0021998317691811>.
- [26] Santana de Vega E, Allegri G, Zhang B, Hamerton I, Hallett SR. Improving the delamination bridging performance of Z-pins through the use of a ductile matrix. *Compos Part A Appl Sci Manuf* 2022;163:107241. <https://doi.org/10.1016/j.compositesa.2022.107241>.
- [27] Huntsman Co. Araldite® LY 3508* / Aradur® 22962* Datasheet 2012:1–5.
- [28] Toyobo Corporation. PBO Fibre Zylon Technical Information. 2005.
- [29] Toray Composite Materials. T300 Standard Modulus Carbon Fiber Datasheet. 2018.
- [30] Hamerton I. On the natural selection of high performance polymers. *Arkivoc* 2021;2021:37–72. <https://doi.org/https://doi.org/10.24820/ark.5550190.p011.517>.
- [31] Iredale RJ. Solvent-free, liquid processable bismaleimide-triazine resins (Thesis). 2019.
- [32] Lander JK. Method of providing through-thickness reinforcement of a laminated material, 2013.
- [33] Yasae M, Mohamed G, Hallett SR. Interaction of Z-pins with multiple mode II delaminations in composite laminates. *Exp Mech* 2016;56:1363–72. <https://doi.org/10.1007/s11340-016-0175-9>.
- [34] Santana de Vega E, Allegri G, Zhang B, Hamerton I, Hallett SR. Improving the delamination bridging performance of fibrous composite Z-pins. *Proc. 20th Eur. Conf. Compos. Mater. Compos. Meet Sustain., vol. 1, 2022, p. 471–8.* https://doi.org/doi:10.5075/epfl-298799_978-2-9701614-0-0.
- [35] Boyce JS, Freitas GA, Magee CL, Fusco TM, Harris JJ, Kunkel E. Ultrasonic fastening system and method, 1998.
- [36] Sweeting RD, Thomson RS. The effect of thermal mismatch on Z-pinned laminated composite structures. *Compos Struct* 2004;66:189–95. <https://doi.org/10.1016/j.compstruct.2004.04.037>.
- [37] Partridge IK, Cartié DDR. Delamination resistant laminates by Z-Fiber® pinning: Part I manufacture and fracture performance. *Compos Part A Appl Sci Manuf* 2005;36:55–64. <https://doi.org/10.1016/j.compositesa.2004.06.029>.
- [38] Zhang B, Allegri G, Hallett SR. An experimental investigation into multi-functional Z-pinned composite laminates. *Mater Des* 2016;108:679–88. <https://doi.org/10.1016/j.matdes.2016.07.035>.
- [39] Greenhalgh ES. Delamination-dominated failures in polymer composites. *Fail Anal Fractography Polym Compos*, Woodhead Publishing 2009:164–237. <https://doi.org/10.1533/9781845696818.164>.
- [40] Zhang B, Allegri G, Yasae M, Hallett SR. Micro-mechanical finite element analysis of Z-pins under mixed-mode loading. *Compos Part A Appl Sci Manuf* 2015;78:424–35. <https://doi.org/10.1016/j.compositesa.2015.07.006>.
- [41] Chang P, Mouritz AP, Cox BN. Properties and failure mechanisms of z-pinned laminates in monotonic and cyclic tension. *Compos Part A Appl Sci Manuf* 2006;37:1501–13. <https://doi.org/10.1016/j.compositesa.2005.11.013>.
- [42] Chang P, Mouritz AP, Cox BN. Flexural properties of z-pinned laminates. *Compos Part A Appl Sci Manuf* 2007;38:244–51. <https://doi.org/10.1016/j.compositesa.2006.05.004>.
- [43] Mouritz AP. Compression properties of z-pinned composite laminates. *Compos Sci Technol* 2007;67:3110–20. <https://doi.org/10.1016/j.compscitech.2007.04.017>.